AD-A066 102 MISSION RESEARCH CORP SANTA BARBARA CALIF F/G 17/2.1
COMPARISON OF SIGNAL SCINTILLATION MODELS.(U)
JUL 78 R C SCOTT, D L KNEPP DNA001-77-C-0096
UNCLASSIFIED MRC-R-406 DNA-4652T NL

| OF |

AD
A066102

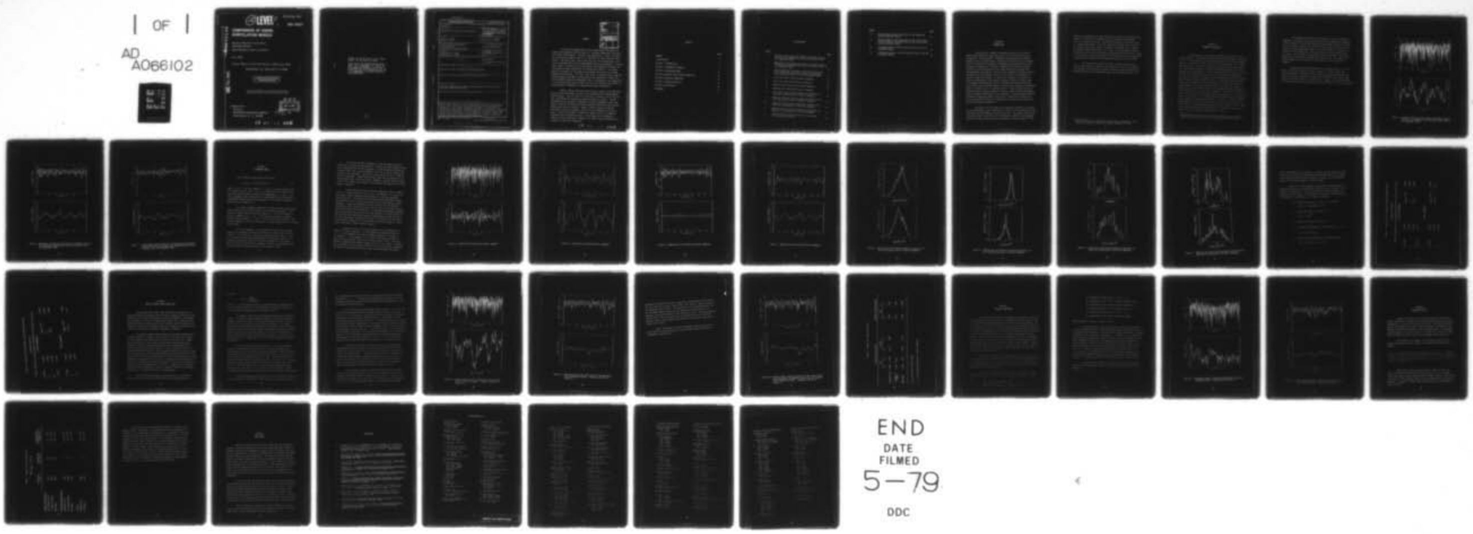

END
DATE
FILMED
5-79
DDC

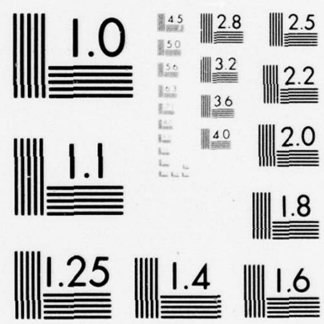

MICROCOPY RESOLUTION TEST CHART

NATIONAL BUREAU OF STANDARDS-1963-A

AD-E300 460

(12) LEVEL III

DNA 4652T

COMPARISON OF SIGNAL SCINTILLATION MODELS

Mission Research Corporation
735 State Street
Santa Barbara, California 93101

July 1978

Topical Report for Period February 1978—June 1978

CONTRACT No. DNA 001-77-C-0096

APPROVED FOR PUBLIC RELEASE;
DISTRIBUTION UNLIMITED.

THIS WORK SPONSORED BY THE DEFENSE NUCLEAR AGENCY
UNDER RDT&E RMSS CODE B322078462 I25AAXYX96001 H2590D.

Prepared for
Director
DEFENSE NUCLEAR AGENCY
Washington, D. C. 20305

Destroy this report when it is no longer needed. Do not return to sender.

PLEASE NOTIFY THE DEFENSE NUCLEAR AGENCY, ATTN: TISI, WASHINGTON, D.C. 20305, IF YOUR ADDRESS IS INCORRECT, IF YOU WISH TO BE DELETED FROM THE DISTRIBUTION LIST, OR IF THE ADDRESSEE IS NO LONGER EMPLOYED BY YOUR ORGANIZATION.

UNCLASSIFIED

SECURITY CLASSIFICATION OF THIS PAGE (When Data Entered)

REPORT DOCUMENTATION PAGE		READ INSTRUCTIONS BEFORE COMPLETING FORM
1. REPORT NUMBER DNA 4652T	2. GOVT ACCESSION NO.	3. RECIPIENT'S CATALOG NUMBER (9)
4. TITLE (and Subtitle) (6) COMPARISON OF SIGNAL SCINTILLATION MODELS,		5. TYPE OF REPORT & PERIOD COVERED Topical Report for Period February 1978—June 1978
		6. PERFORMING ORG. REPORT NUMBER (14) MRC-R-406
7. AUTHOR(s) (10) Richard C. Scott Dennis L. Knepp		8. CONTRACT OR GRANT NUMBER(s) (15) DNA 001-77-C-0096
9. PERFORMING ORGANIZATION NAME AND ADDRESS Mission Research Corporation 735 State Street Santa Barbara, California 93101		10. PROGRAM ELEMENT, PROJECT, TASK AREA & WORK UNIT NUMBERS Subtask I25AAXYX960-01 (16)
11. CONTROLLING OFFICE NAME AND ADDRESS Director Defense Nuclear Agency Washington, D.C. 20305		12. REPORT DATE (11) July 1978 (17) X960
		13. NUMBER OF PAGES 48
14. MONITORING AGENCY NAME & ADDRESS(if different from Controlling Office) (12) 48p.		15. SECURITY CLASS (of this report) UNCLASSIFIED
		15a. DECLASSIFICATION DOWNGRADING SCHEDULE

16. DISTRIBUTION STATEMENT (of this Report)

(18) DNA, SBIE

Approved for public release; distribution unlimited.

(19) 4652T, AD-E300 460

17. DISTRIBUTION STATEMENT (of the abstract entered in Block 20, if different from Report)

18. SUPPLEMENTARY NOTES

This work sponsored by the Defense Nuclear Agency under RDT&E RMSS Code B322078462 I25AAXYX96001 H2590D.

19. KEY WORDS (Continue on reverse side if necessary and identify by block number)

20. ABSTRACT (Continue on reverse side if necessary and identify by block number)

Scintillating signals taken from the DNA Wideband satellite experiment are used as direct input to a digital simulation of a phase-shift keyed (PSK) demodulator. The resulting demodulator performance is compared to that obtained with input signals generated according to a two-component (log-normal plus joint Gaussian) model. A second comparison is made with input signals generated by a multiple phase screen propagation simulation. Results are used to assess the suitability of the models for simulation of satellite communication systems in disturbed environments.

DD FORM 1 JAN 73 1473 EDITION OF 1 NOV 65 IS OBSOLETE

UNCLASSIFIED

SECURITY CLASSIFICATION OF THIS PAGE (When Data Entered)

406 548

LB

SUMMARY

Scintillating communication signals generated by two models are compared with Wideband satellite data in a simulated demodulator for phase-shift keyed (PSK) signals. To effect this comparison, a digital simulation of a PSK modem designed for DSCS II is exercised for three different input signals. One input signal, which forms the basis for the comparison, consists of detrended data from the DNA Wideband satellite experiment. A second input signal is obtained from the statistical two-component log-normal plus joint-gaussian model proposed by SRI International (SRII).[1] The initial statistics required for this model are obtained from analysis of the DNA Wideband satellite data. The final input signal is obtained from a numerical multiple phase-screen (MPS) simulation which was generated to "match" the initial Wideband satellite experimental data. The purpose of the comparisons is to test the capabilities of models now in use to represent the effects of transionospheric propagation in communication system simulations.

Results indicate that both the statistical model and the MPS model yield receiver performance similar to that obtained with the DNA Wideband satellite data. Thus, at least for this class of receiver and for PSK signals, both methods of generating simulated signals are useful. The MPS simulation has the potential advantage of yielding information about ionospheric structure including rms electron-density fluctuations and electron-density power spectral density. However, the MPS simulation requires information on the link geometry as well as the ionospheric structure as input. The major advantage of statistical models, such as the combined log-normal and joint-gaussian model, is the simplicity of generating signals with such statistics. However, such models require information on a number of statistical parameters.

CONTENTS

ILLUSTRATIONS

FIGURE		PAGE

SECTION 1
INTRODUCTION

Satellites have assumed an important position in the overall communication capability supporting both civil and military operations. Consequently, transionospheric propagation considerations have become a necessary part of system design. Experience has shown that the ionosphere cannot be considered a transparent, homogeneous propagation medium, even at gigahertz frequencies.[2-4] Design of communication signals and signal processors requires knowledge of the signal distortion resulting from transionospheric propagation. Models of the ionospheric distortion process are needed for these designs and to test the results of propagation on specific signals and systems. A further use of models is to serve as a basis for extrapolation from natural ionospheric effects to effects due to ionospheric perturbations caused by high altitude nuclear explosions. Since little data on nuclear induced scintillation is available, propagation models must be derived on a theoretical basis. These models should, as a minimum, properly predict propagation effects through a natural ionosphere, given an adequate description of the ionosphere. The development of transionospheric propagation models, then, leads to derivation of models for use in design and simulation of communication systems and to extraction of pertinent ionospheric parameters.

The purpose of this study is to compare the results of two models for transionospheric signal scintillation. The basis for comparison is data taken from the DNA Wideband satellite experiment.[1] The models used are the 2-component model[5] developed at SRI International (SRII), and the multiple phase screen (MPS) numerical Fourier propagation simulation model.[6,10] For

purposes of comparison, two time periods were selected from Wideband data taken at Ancon, Peru, on December 16, 1976, and kindly furnished by Mr. R. C. Livingston of SRII. Selections were made on the basis of the S_4 scintillation index. The first time period extends over a period of 40 seconds, starting at 4 hours, 47 minutes, 32 seconds (UT).* During this period signal scintillation was severe. The scintillation index at 413 MHz was 1.00, and at 1239 MHz the scintillation index was 0.45. During this period only the last 30 seconds of 1239 MHz data was used because the L-band signal was used for phase reference during the first 10 seconds.

The second time period, taken from the same satellite pass, extends from 4 hours, 49 minutes, 48.6 seconds, to 4 hours, 50 minutes, 28.6 seconds, and illustrates a period of moderate signal scintillation. During this period the scintillation index for the UHF signal was 0.56.

---

* Local time at Ancon is five hours earlier than at Greenwich. Local time was 23 hours, 47 minutes, 32 seconds, December 15, 1976.

SECTION 2
PARAMETER ESTIMATION

Experimental data is recorded as quadrature components of the received signal. The Wideband beacon provides an S-band signal (2891.2 MHz) for use as a phase reference for coherent detection of the lower frequency signals. The satellite signal received on the ground would vary in amplitude and phase as a result of changing slant range, antenna gain pattern, and total electron content (TEC) along the propagation path, even if the ionosphere were unperturbed. As the satellite progresses through the pass, the line from satellite to receiver scans a portion of the ionosphere. The process of scanning translates spatial ionospheric variations into temporal variations of the received signal. The variations discussed above, resulting from conditions of the experiment, take place slowly and are termed trends. The initial processing step is to remove the trends. In Reference 5, Fremouw and Rino discuss the detrending process and adopt an upper frequency of 0.1 Hz for trend components. This limit was found by use of the criterion that detrending should not reduce the S_4 index by more than "a few" percent. It is clear that this frequency limit is dependent on the geometry of the propagation path.* It is also very likely that it should depend on ionospheric structure. For this work we have used the 0.1 Hz cutoff, 6 pole Butterworth numerical filter adopted by SRII. Signal level variations with periods greater than ten seconds are normally of little concern in operational communication systems.

---

* Reference 5 reports detrending ATS-6 data with filter time constants sixty times as long as those used for Wideband and Transit data.

The Wideband satellite data is presented in terms of quadrature components. The phase of the signal derived from the quadrature components is made continuous by limiting the phase change between consecutive samples to plus or minus π radians. The intensity of the signal is the sum of the squares of the component amplitudes. Phase and logarithm of intensity are low-pass filtered separately. The filter output is then subtracted from the input. In this manner log-intensity and phase variations with periods greater than ten seconds are removed from the raw data. The subtraction process normalizes the intensity by the average over the filter time constant.

Detrended amplitude and phase for the Wideband signals at 413 MHz and at 1239 MHz are shown in Figures 1 through 3. Figure 1 shows the detrended intensity and phase for the earlier, severely scintillating, UHF signal and Figure 2 presents the moderately scintillating UHF signal during the 40 second period about two minutes later. Figure 3 shows the detrended L-band signal during the time period when the UHF signal is severely disturbed.

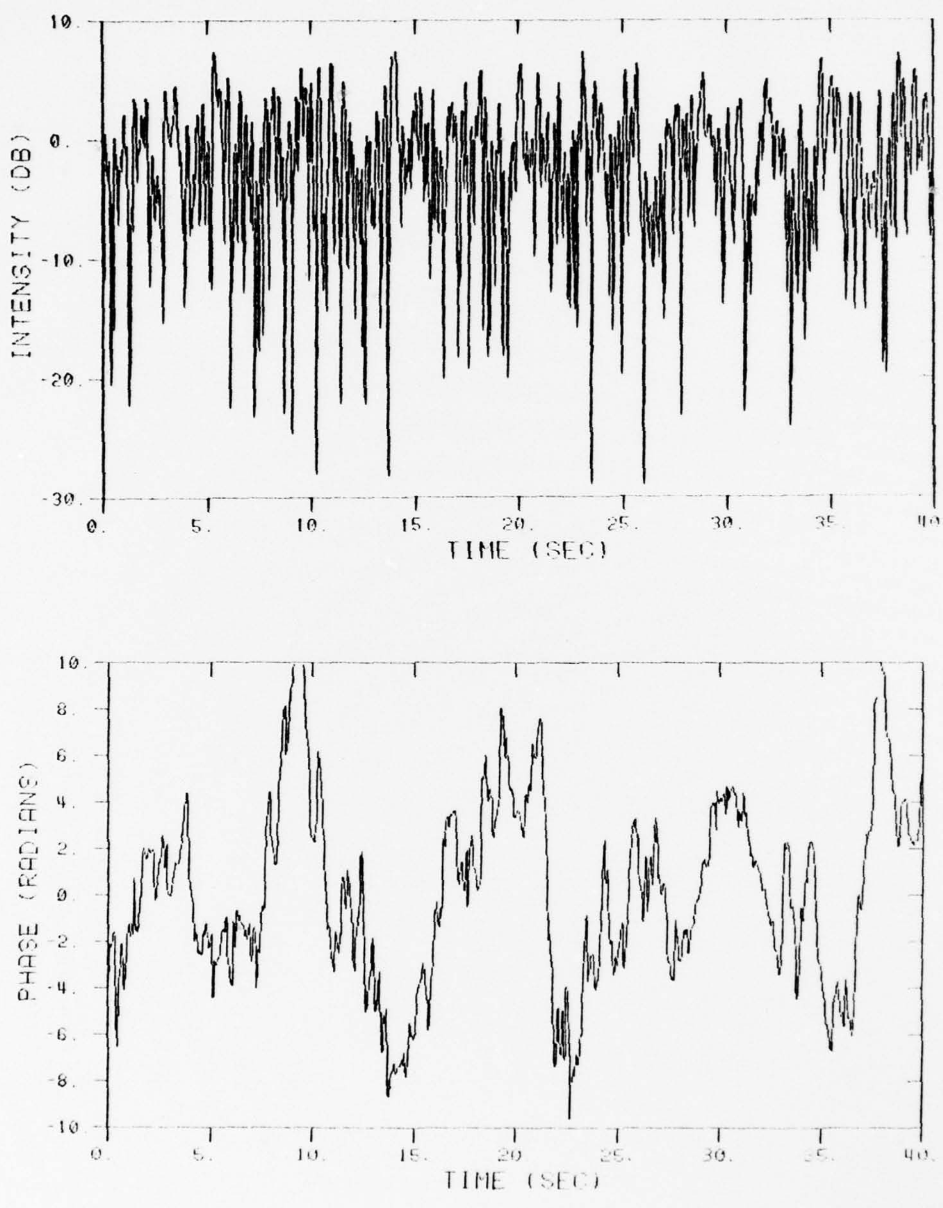

Figure 1. Severely scintillating UHF signal—(detrended intensity and phase from Wideband satellite pass at Ancon, Peru, on 16 December 1976).

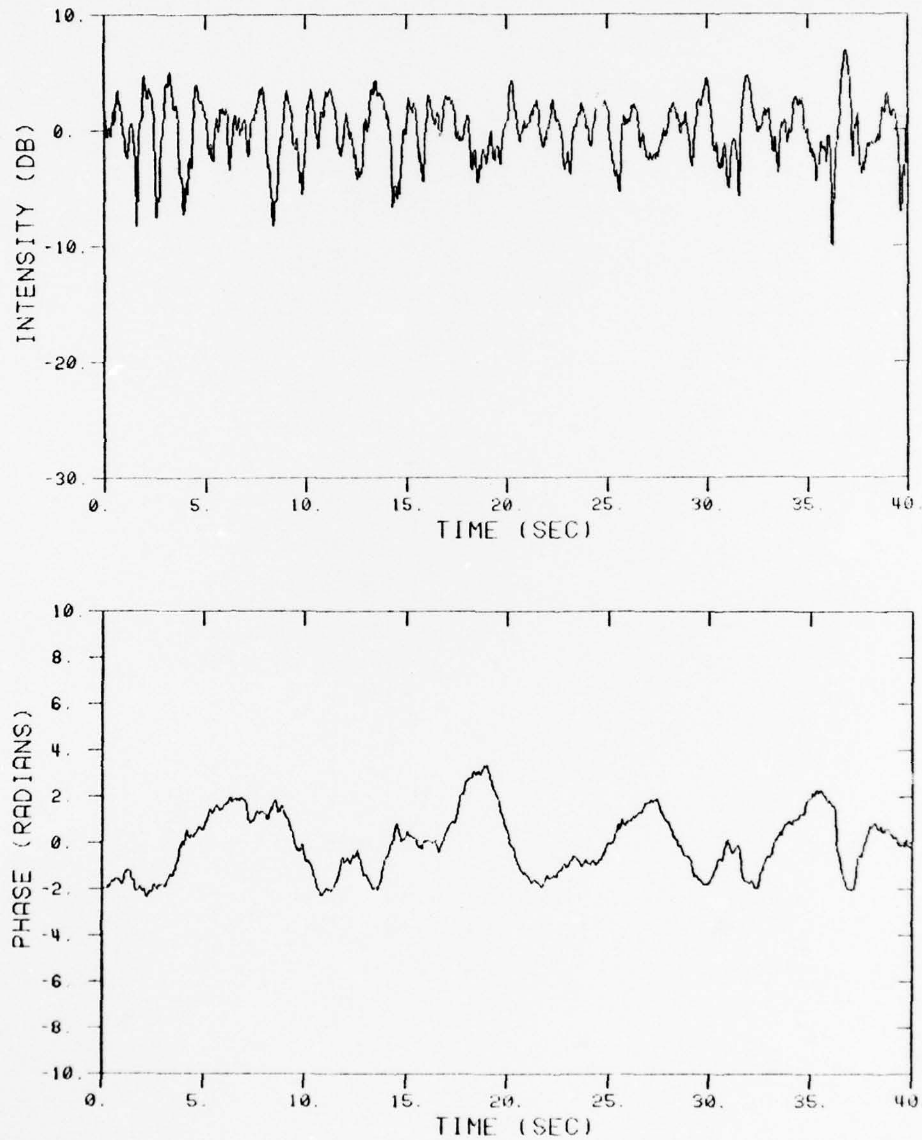

Figure 2. Moderately scintillating UHF signal—(detrended intensity and phase from Wideband satellite pass at Ancon, Peru, on 16 December 1976).

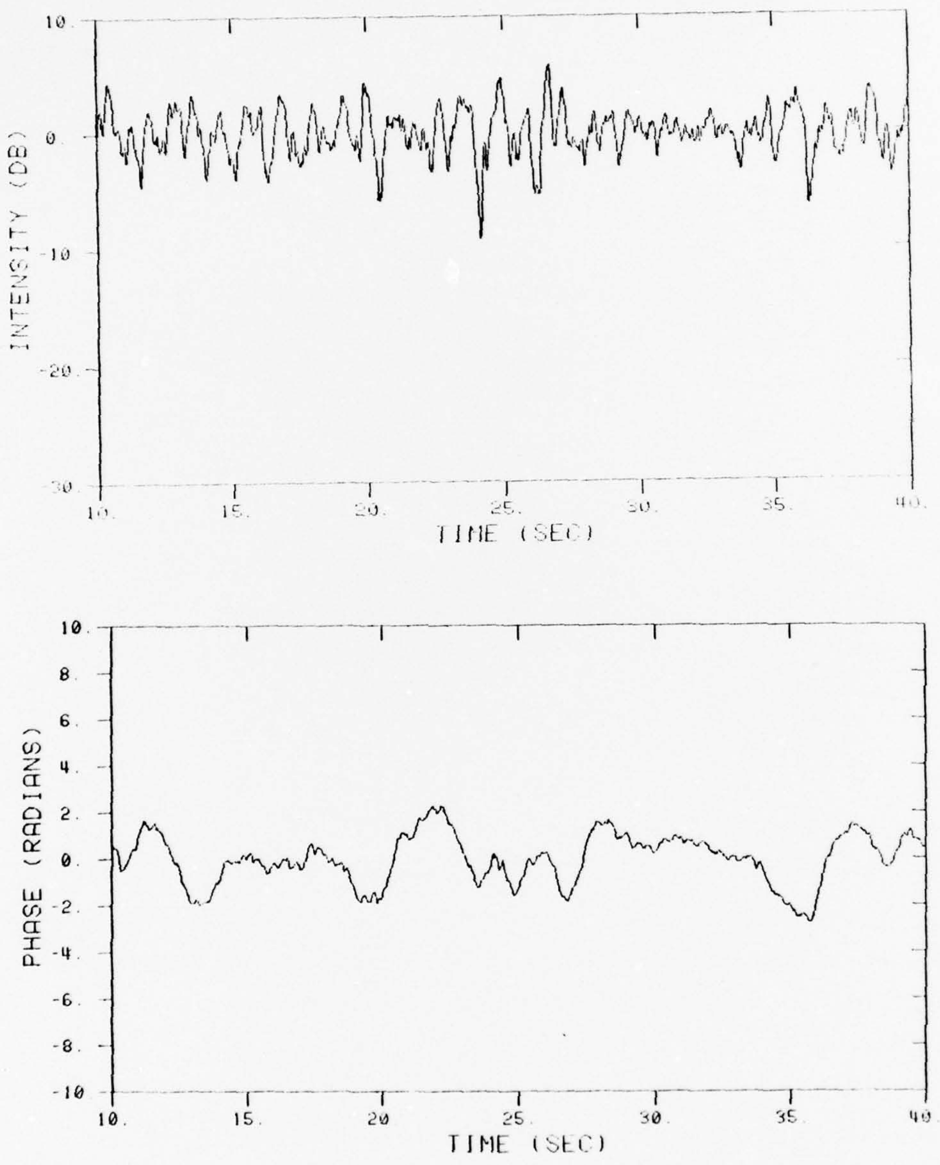

Figure 3. L-band signal during severely scintillating UHF conditions—(detrended intensity and phase from Wideband satellite pass at Ancon, Peru, on 16 December 1976).

SECTION 3
2-COMPONENT MODEL

The 2-component signal model has the form

$$E = E_s E_f = (\mu + x + jy)\exp(\eta + \chi + j\phi) \quad , \qquad (1)$$

where μ and η are real constants, x and y are joint gaussian zero mean random variables, and χ and ϕ are another pair of joint gaussian zero mean random variables statistically independent of x and y. In this 2-component model scintillation is represented by two statistically independent multiplicative random components: the "scatter" component E_s, and the "focus" component, E_f.

The scatter component represents the rapidly varying signal amplitude and phase caused by fairly small-scale ionization structure. It is modeled by complex gaussian statistics wherein μ is the unscattered or specular component, and x and y are a pair of correlated zero-mean gaussian random variables. x and y need not have equal variances. This scatter component is associated with what is sometimes referred to as classical scintillation.

The focus component, E_f, represents the more slowly varying components of amplitude and phase caused by fairly large-scale ionization structure. It is modeled by complex log-normal statistics where χ and ϕ are correlated zero-mean random variables with unequal variances. The amplitude fluctuations associated with this component are often rather small; the primary effect of this component is usually associated with the relatively slowly fluctuating phase of the composite signal.

The scatter and focus components of the detrended signal are separated in a second filtering process. Because this model assumes statistical independence of the two components, a 10-pole Butterworth numerical low-pass filter with a cutoff frequency of 0.4 Hz is used to separate the spectra of the components. The output of the low-pass filter is taken as the focus component. Subtracting the focus phase and log intensity from the detrended signal gives the scatter component. Scatter and focus components of the severely and moderately scintillating UHF signals are given in Figures 4 through 7.

The gaussian nature of the scatter component is shown in Figures 8 and 9. In these figures the real $(\mu+x)$ and imaginary (y) parts of the complex scatter component are presented as a discrete probability density function. The normalization performed during detrending divides the amplitude terms by the root mean square of the total received signal amplitude. A gaussian probability density function with the mean and standard deviation calculated from the data for each case is plotted with the discrete function for comparison. We note that the imaginary component has an essentially zero mean for both time segments for the UHF signal. In the severely scintillating UHF signal the normalized real part has a mean of 0.28, approaching a Rayleigh distribution. The mean of the real part of the scatter component for the moderately scintillating signal is nearly unity, indicating a largely specular process.

Figures 10 and 11 show the distributions of the amplitude and phase of the focus component. In these figures the normalized value of $\eta + \chi$ is the logarithm of the focus component amplitude. The phase is the quantity ϕ from Equation 1. The discrete distribution functions plotted in these figures suffer from a limited amount of data. The focus spectral components have periods ranging from 2.5 to 10 seconds. Therefore, the 40 seconds of data used here contain 4 to 16 cycles of these components. The spikes in the density functions clearly match the maxima and minima

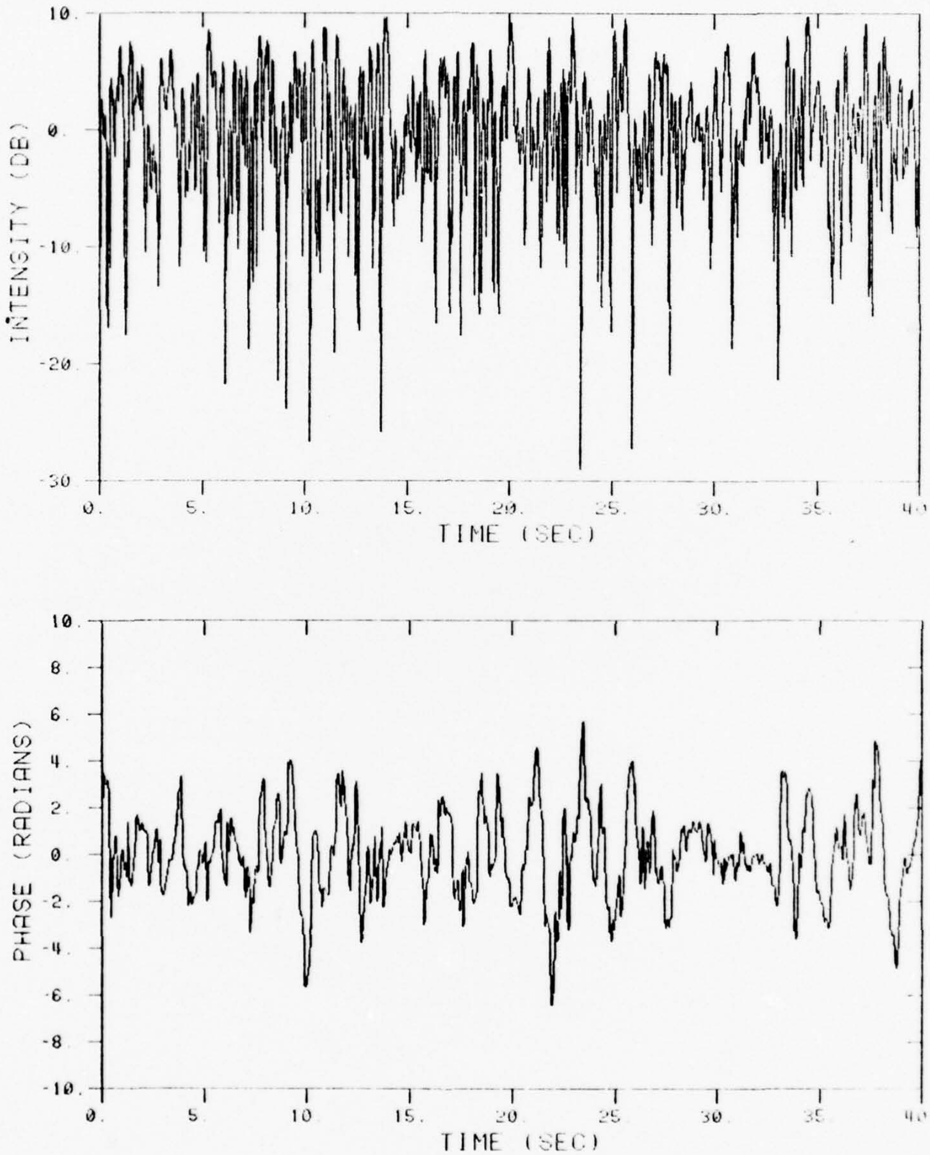

Figure 4. Severe UHF scintillation—scatter component.

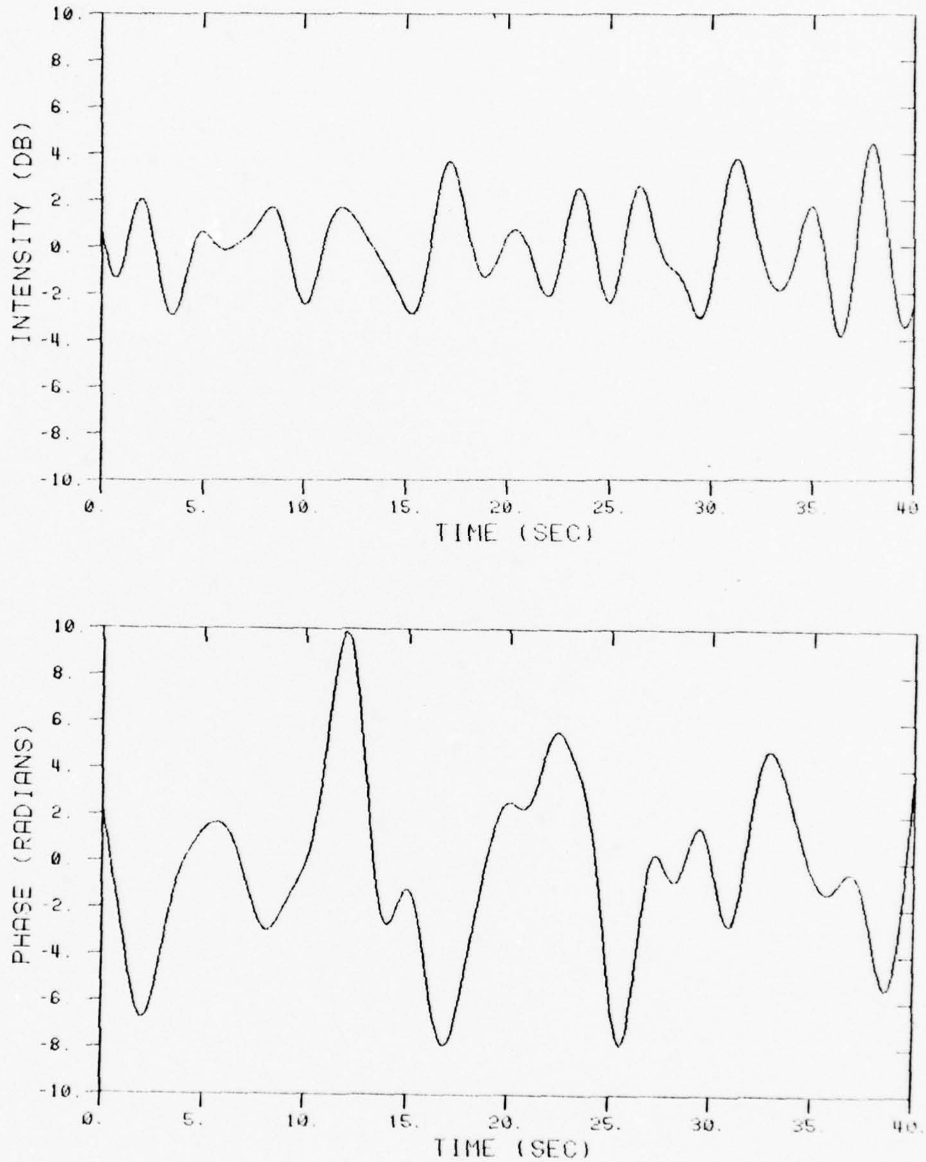

Figure 5. Severe UHF scintillation—focus component.

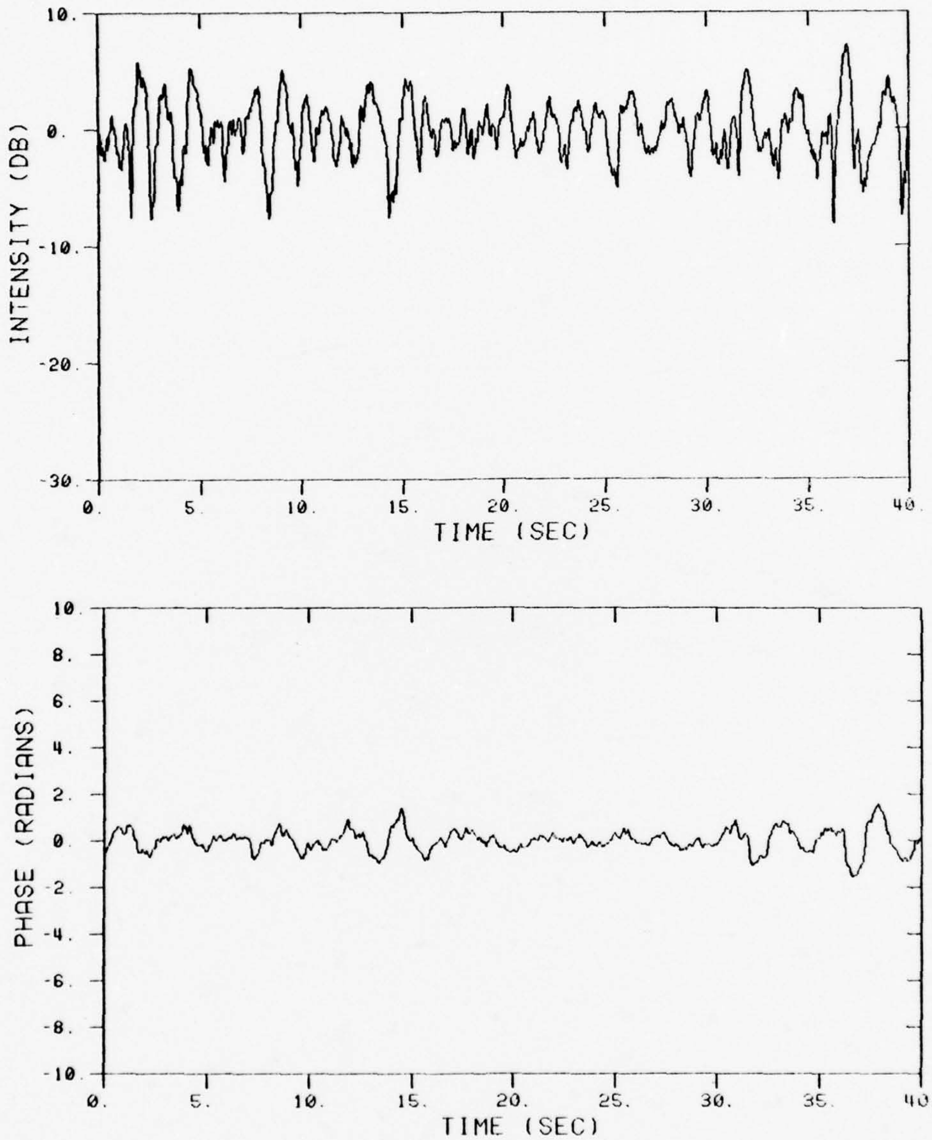

Figure 6. Moderate UHF scintillation—scatter component.

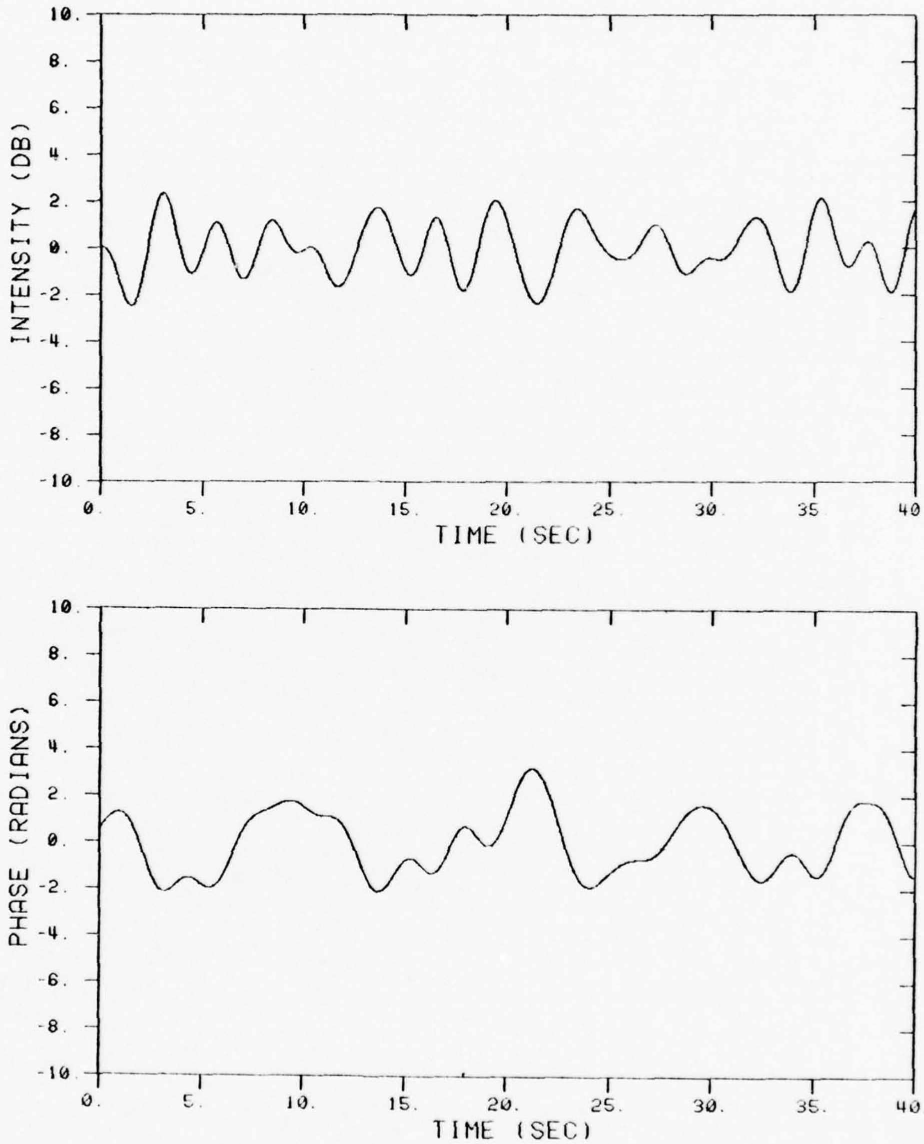

Figure 7. Moderate UHF scintillation—focus component.

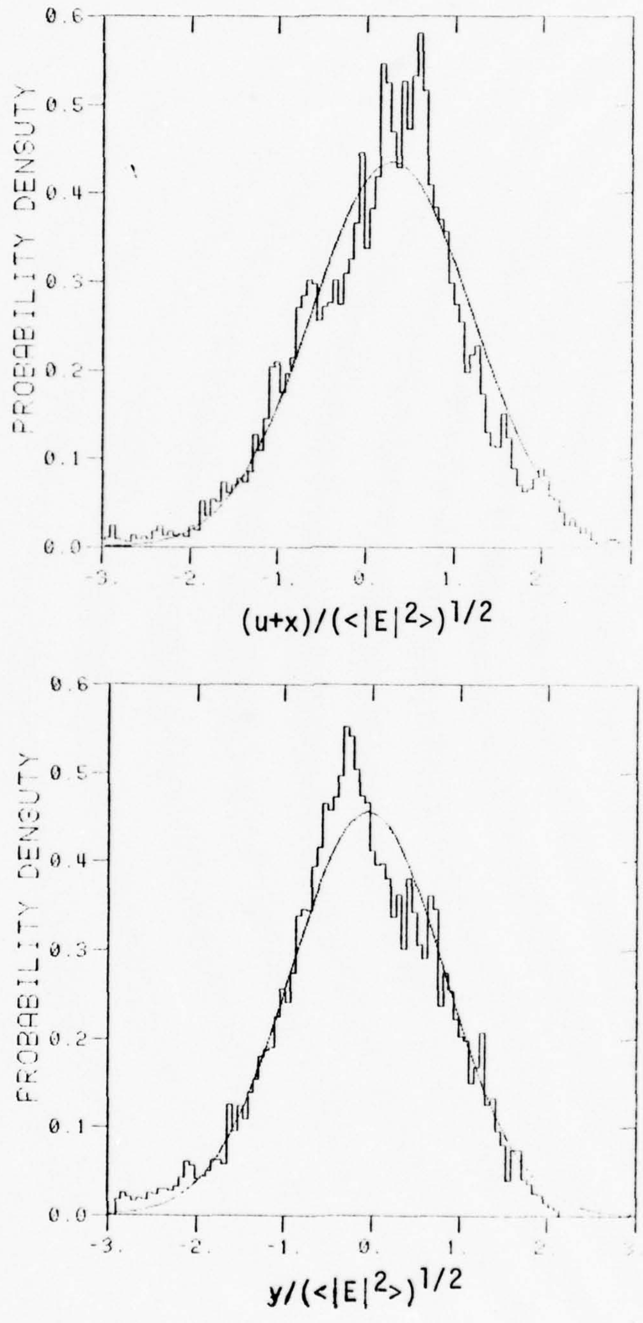

Figure 8. Severe UHF scintillation—probability densities for real and imaginary parts of scatter component.

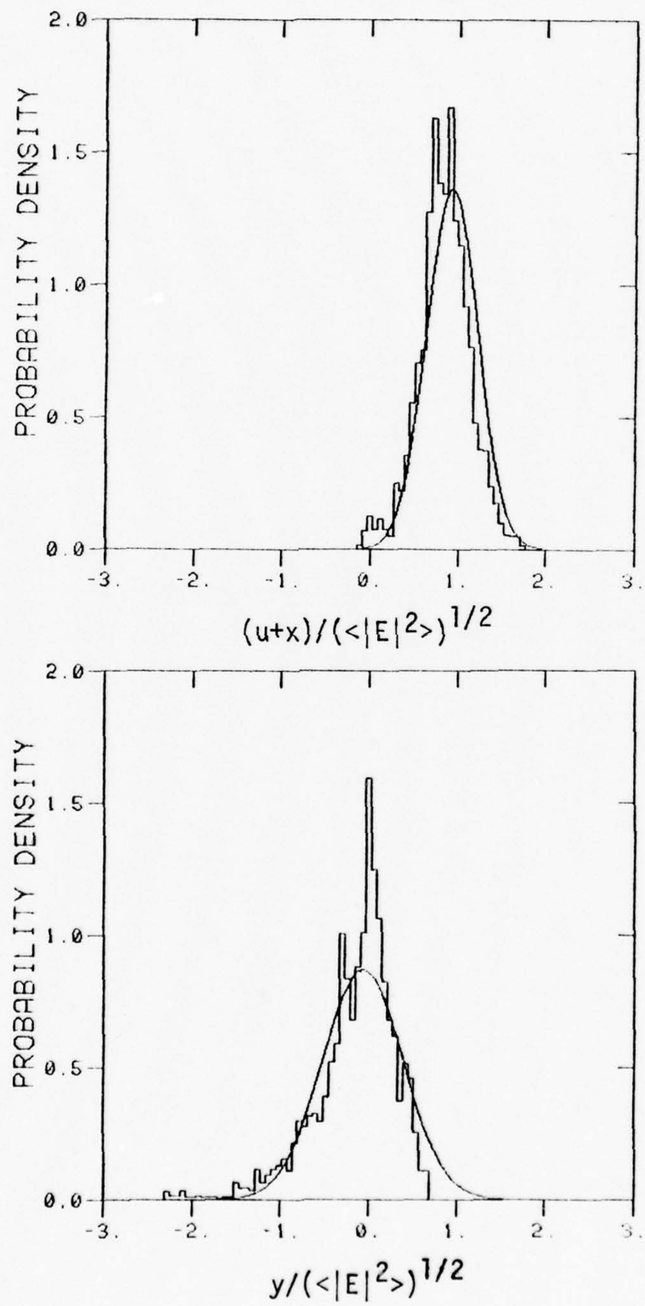

Figure 9. Moderate UHF scintillation—probability densities for real and imaginary parts of scatter component.

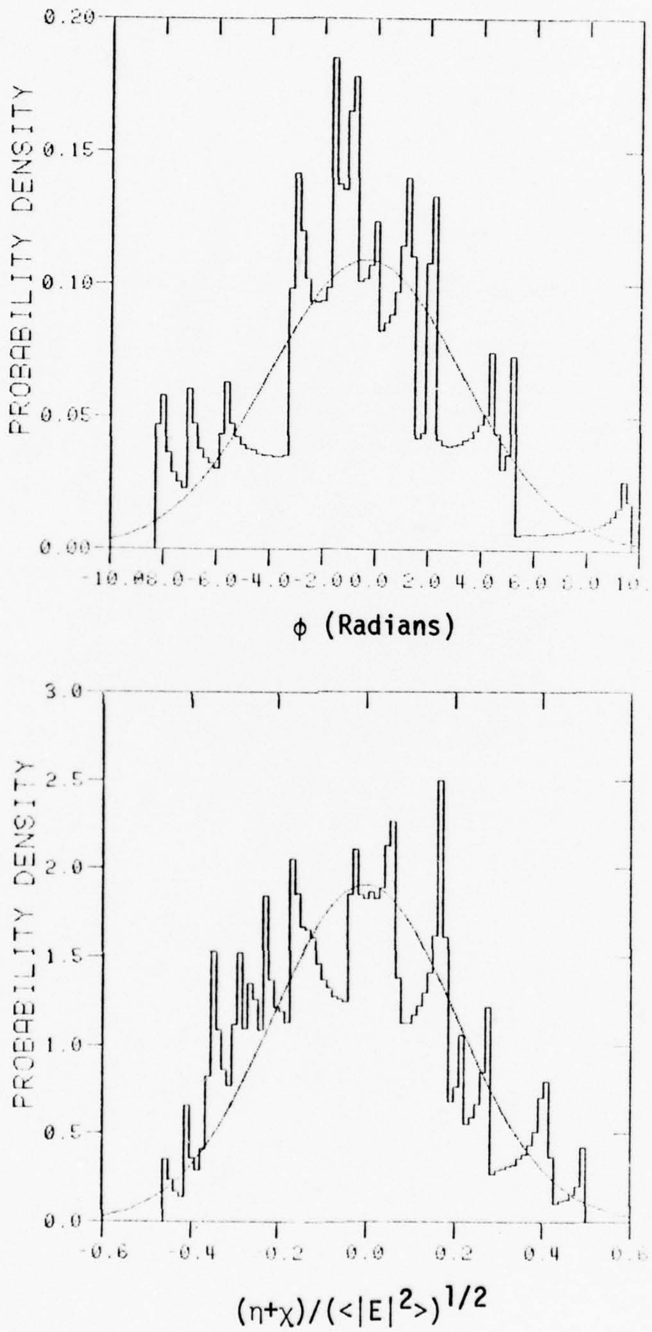

Figure 10. Severe UHF scintillation—probability densities for phase and log-amplitude of the focus component.

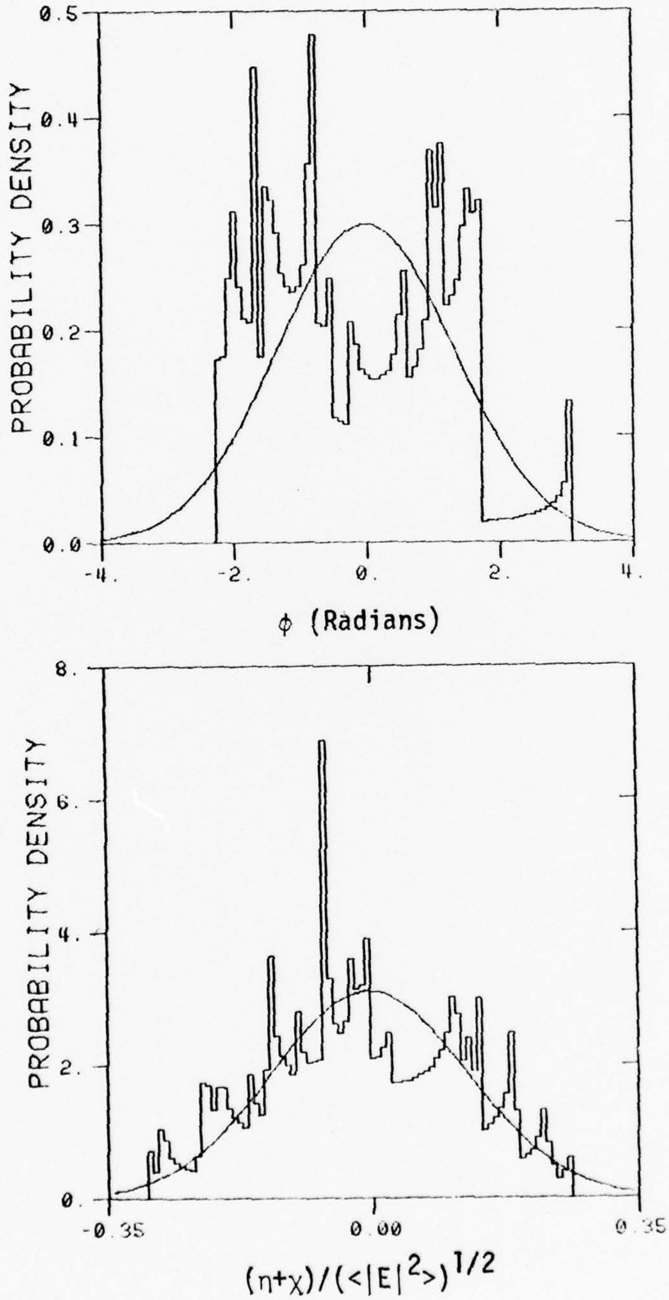

Figure 11. Moderate UHF scintillation—probability densities for phase and log-amplitude of the focus component.

of the corresponding time functions. It appears that the discrete density functions would as likely approach gaussian distributions with zero means as any other distribution if more data were included in the calculation. This is true for both segments of the UHF signal.

Statistics for the detrended, normalized, continuous phase UHF signals during the two 40 second time periods are given in Tables 1 and 2. Each set of statistics is a result of processing 20,000 samples of the Wideband satellite signal. The parameters in the table are defined below for reference. Angle brackets, <>, indicate averages.

$$S_4 = \text{Scintillation index} = [(\langle I^2\rangle - \langle I\rangle^2)/\langle I\rangle^2]^{1/2}$$

where I is intensity $= |E|^2$

$$\sigma_x = \text{Root mean square of values of } x$$

$$= [\langle x^2\rangle - \langle x\rangle^2]^{1/2}$$

$$\sigma_y = \text{Root mean square of values of } y .$$

$$\rho_{xy} = \text{Normalized coefficient of correlation of } x \text{ and } y$$

$$= \langle (x-\langle x\rangle)(y-\langle y\rangle)\rangle/\sigma_x\sigma_y$$

$$\tau_x = \text{Time interval such that the correlation between}$$

$$x(t) \text{ and } x(t+\tau) = 1/e = 0.37$$

Table 1. Statistics for severely scintillating UHF signal.

Wideband satellite

Data at Ancon, Peru, during period 23:47:32 to 23:48:12 local time.

SCATTER COMPONENT

S_4 Index	0.9825	σ_{phase} (rad)	1.8456
σ_x	0.9164	σ_y	0.8756
ρ_{xy}	- 0.0022	σ_x^2/σ_y^2	1.0952
τ_s (sec)	0.12		

FOCUS COMPONENT

S_4 Index	0.4416	σ_{phase} (rad)	3.6563
σ_χ	0.2090	τ_F (sec)	10.0
$\rho_{\chi\phi}$	- 0.1376		

Table 2. Statistics for moderately scintillating UHF signal.

Wideband satellite

Data at Ancon, Peru, during period 23:49:48.6 to 23:50:28.6 local time.

SCATTER COMPONENT

S_4 Index	0.5920	σ_{phase} (rad)	0.4642
σ_x	0.2922	σ_y	0.4585
ρ_{xy}	- 0.2039	σ_x^2/σ_y^2	0.4061
τ_s (sec)	0.325		

FOCUS COMPONENT

S_4 Index	0.2569	σ_{phase} (rad)	1.3328
σ_χ	0.1282	τ_F (sec)	10.0
$\rho_{\chi\phi}$	- 0.5435		

SECTION 4
MULTIPLE PHASE SCREEN SIMULATION

The multiple phase screen (MPS) propagation simulation is an analytical/numerical technique which provides a numerical solution for the propagation of a plane wave through a disturbed ionosphere. By modeling the ionosphere as a series of random phase screens with a power-law power spectral density and utilizing the actual Wideband satellite geometry, we attempt to "match" the experimental data (in a qualitative sense) and thus obtain some information on possible ionospheric parameters.

The multiple phase-screen propagation simulation represents the disturbed region by a number of phase-screens (10 for this work) located in the disturbed region between the satellite and the receiver. Random phase fluctuations in each screen are generated using the statistical properties of the electron-density fluctuations as determined by the electron-density power spectral density. A wave (initially plane as it enters the disturbed region) is then propagated numerically from one screen to the next by use of the Fresnel-Kirchhoff integral equation until a solution is obtained for the complex electric field in the receiver plane. This technique is equivalent to a solution of the parabolic wave equation and is thus able to account for multiple scattering.[8] Since the phase-screens are random, the signal propagated to the receiver is random and, if desired, statistics may be obtained by averaging a number of different simulations, each based on a different sequence of random numbers.

The electron-density power spectral density is a simulation input, but here we assume a one-dimensional power spectral density of

the form

$$S(K_\perp) = \frac{\sigma_N^2 L_o}{\pi(1+K_\perp^2 L_o^2)}$$

where σ_N is the standard deviation of electron-density fluctuation and L_o is the outer scale size. Both parameters are simulation inputs. $K_\perp$ is the wavenumber perpendicular to the magnetic field.

We assumed a 100 km thick ionosphere centered at an altitude of 350 km. To model the actual propagation geometry for the link from the Wideband satellite to Ancon we used constant elevation angles of 15° and 30° for the first and second time periods, respectively. The actual satellite elevation angles were changing slowly during the 40 second time intervals and the use of constant angles simplifies the analysis. In this manner we modeled the early time geometry by a layer of irregularities 386 km thick with the center 1352 km from the receiver. In the late time period the layer of irregularities was 200 km thick centered 700 km from the receiver.

The best match of MPS calculated data to the actual Wideband satellite experimental data was obtained by a visual examination of a small number of plots of intensity and phase generated by the MPS propagation simulation. For both time periods we found that an outer scale size of 500 meters gave reasonable fits to the data. During the first time period an electron density standard deviation of 9.9×10^4 cm^{-3} was used; during the second time period an electron density standard deviation of 3.3×10^4 cm^{-3} was found to give a good fit to the experimental data. Values for both the outer scale size and the electron density standard deviation are within ranges regularly observed in the equatorial ionosphere.

Since the propagation simulation results are functions of distance in a plane normal to the magnetic field direction, the simulation results

may be converted to functions of time by dividing the simulation computed distances by V . V is defined as the component of the velocity at the ionospheric penetration point of the propagation path perpendicular to the local magnetic field direction.

For the strong UHF scintillation case a value of V of 780 m/sec was required to match the observed signal intensity decorrelation time. A value of V of 720 m/sec was required to match the intensity decorrelation time observed for the moderate UHF scintillation. The geometry of the satellite pass indicates that a value of V of about 500-700 m/sec results from satellite motion perpendicular to the magnetic field direction. Another 100-200 m/sec could be added from mean atmospheric drift.[2] These considerations indicate a likely range of V from 600-900 m/sec. The values used here are within this range. The purpose of the comparison is to investigate adequacy of the statistical signal description in the two models—thus, correspondence of subsidary quantities such as V , while encouraging indicators of validity for MPS, are not necessary to a valid comparison.

Note that the simulation parameters which match the Wideband experimental data are not unique. They were chosen simply because they yielded the closest match to the observed signal intensity and phase from a small set of simulations. A somewhat better match may be obtained for a different electron-density standard deviation and outer scale size. However, the signals already obtained seem to match the data quite well and we do not expect that better matches will result in much change in either electron-density standard deviation or outer scale size.

The magnitude and phase of the MPS realizations for the early time period are shown in Figure 12. These can be compared with the corresponding detrended Wideband satellite data in Figure 1. Similarly, the MPS generated amplitude and phase for the late time period are presented in Figure 13 for comparison with Figure 2. In addition, the selected

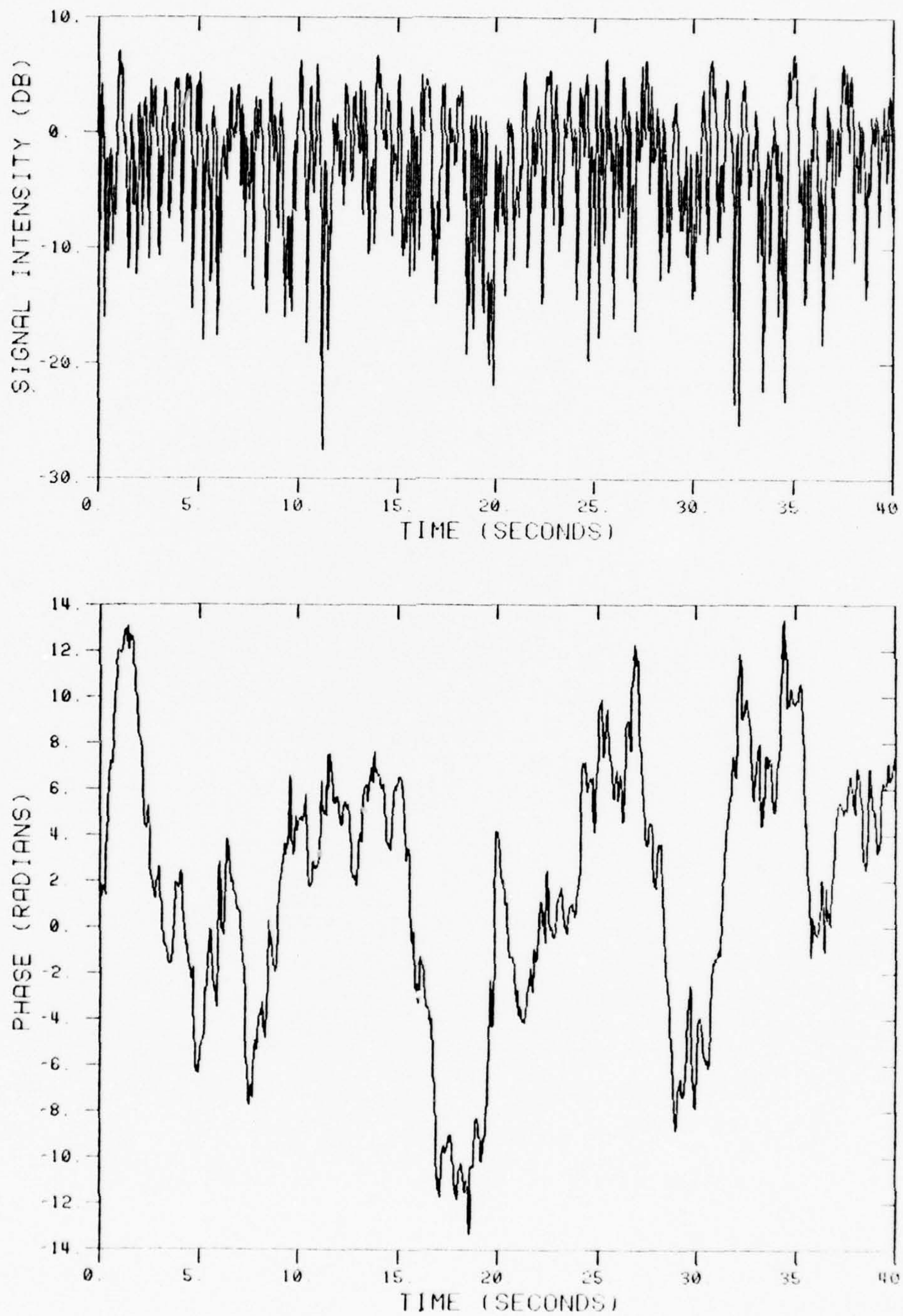

Figure 12. Multiple phase screen realization of the severely scintillating UHF signal. (Compare with data in Figure 1.)

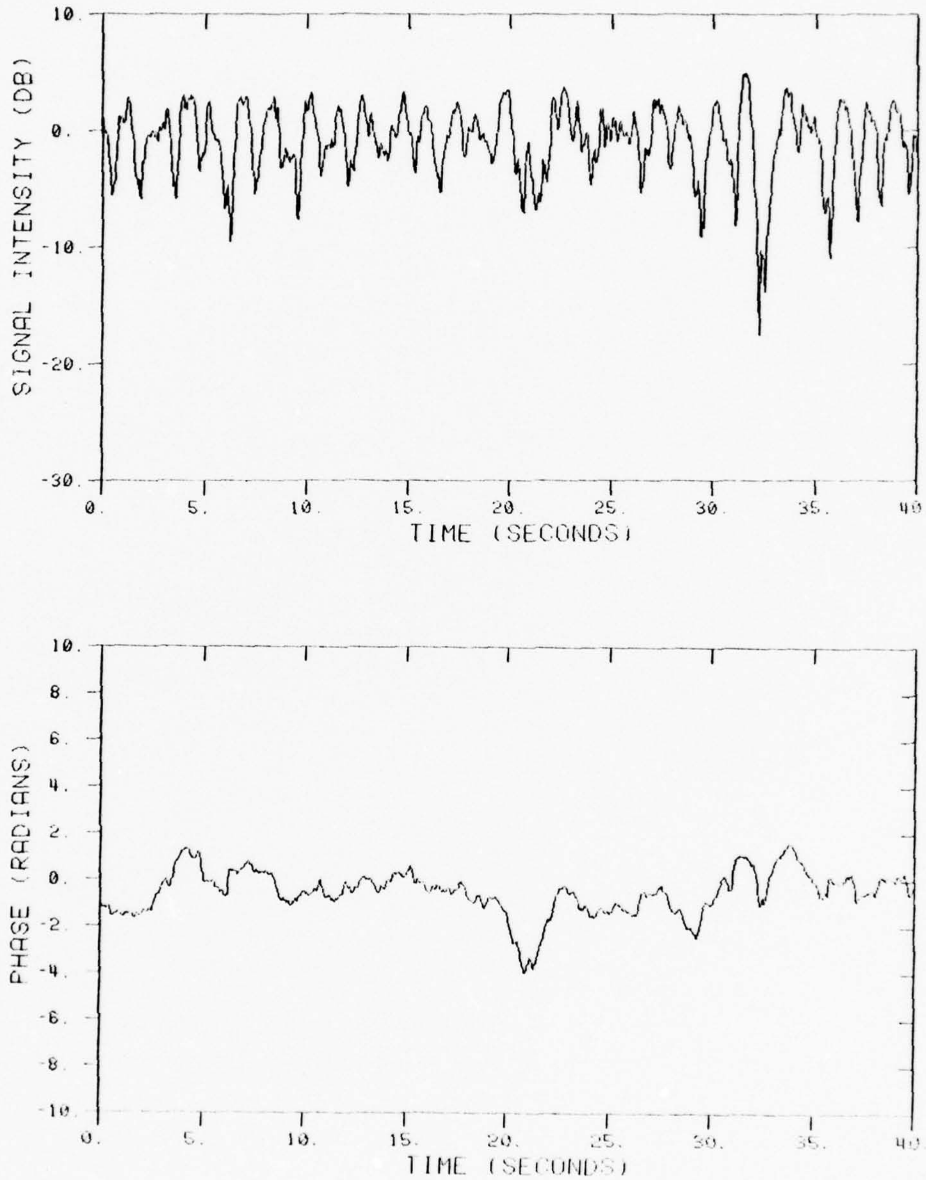

Figure 13. Multiple phase screen realization of the moderately scintillating UHF signal. (Compare with data in Figure 2.)

ionospheric parameters were used to generate a scintillating signal simulation at L-band for the early time period. This signal is shown in Figure 14 for comparison with Figure 3. The similarity of the L-band MPS results and the detrended Wideband satellite data demonstrates the feasibility of modeling scintillation effects at SHF given data at UHF. L-band propagation effects for the late time period were not modeled because the relatively moderate effects at UHF indicate that effects of the L-band signal perturbation will be small.

Table 3 summarizes statistical parameters indicating severity of scintillation for the Wideband data and for signals generated using the 2-component and MPS models.

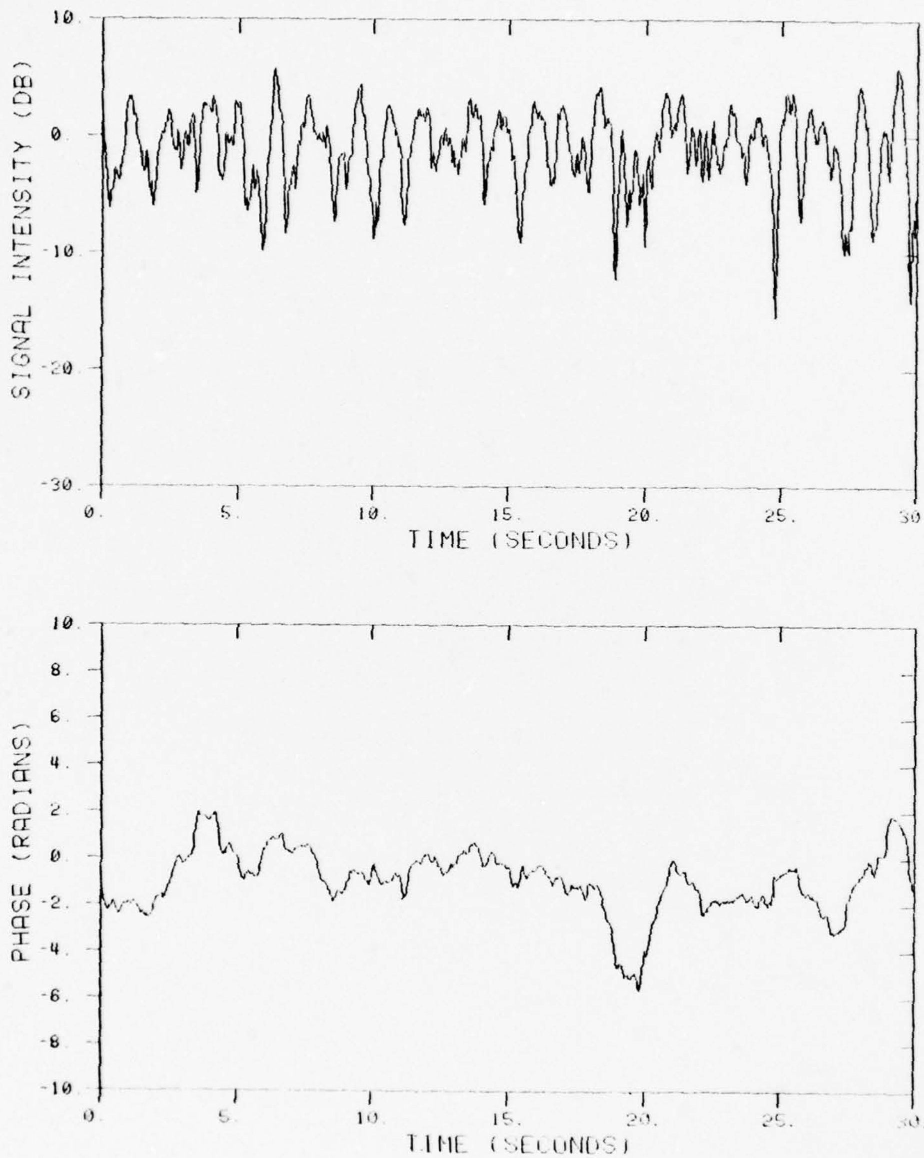

Figure 14. Multiple phase screen realization of the L-band signal using ionospheric parameters derived from the severely scintillating UHF signal. (Compare with data in Figure 3.)

Table 3. Summary of signal statistics.

	SEVERE SCINTILLATION				MODERATE SCINTILLATION	
	UHF		L-Band		UHF	
	S_4	σ_ϕ	S_4	σ_ϕ	S_4	σ_ϕ
Wideband Data	0.998	4.065	0.447	1.059	0.554	1.355
2-Component Model	1.073	20.45			0.571	1.091
MPS Model	0.950	5.625	0.644	1.333	0.555	0.9372

S_4 is the scintillation index.

σ_ϕ is the standard deviation of phase (radians).

SECTION 5
RECEIVER SIMULATION

To investigate the effects of propagation disturbance modeling on the performance of system models, the perturbed signals were used as input to a sampled data digital simulation of the DSCS-II AN/USC-28 modem.[7] For this purpose a 75 bit per second data rate was used with coherent detection of a phase-shift keyed (PSK) signal with differential encoding of the data. The receiver representation used a second order modified Costas phase-locked loop with a loop bandwidth of 21 Hz. The simulation sampling rate was 300/sec. A mean carrier-power-to-noise density of 35 db-Hz, corresponding to a mean E_b/N_o of 16 db was used so that detection errors could be attributed to the nature of the signal rather than to receiver noise. Without signal disturbances the error rate is vanishingly small for this signal-to-noise ratio. The receiver model can accept signal input data in each of the three forms discussed here.

The form of the direct data input to the receiver model consists of digitized amplitude and phase samples. Since the Wideband satellite data is sampled at a rate of 500 samples/second and the receiver model sample rate is 300 samples/second, an interpolation is necessary. Otherwise the detrended data is used directly.

Use of the 2-component model requires that statistics for the scintillating signal be derived. Eight parameters are required. These are:

- Scatter scintillation index, S_4
- Ratio of variances of x and y, σ_x^2/σ_y^2

- Correlation coefficient of x and y , ρ_{xy}
- Decorrelation time (e^{-1}) for the scattered signal, τ_s
- Standard deviation of the log-normal amplitude, σ_χ
- Standard deviation of the log-normal phase, σ_ϕ
- Correlation coefficient of χ and ϕ , $\rho_{\chi\phi}$
- Decorrelation time for the log-normal signal, τ_f

These quantities are given in Tables 1 and 2.

The random scatter signal scintillation components are computed at each sampling time using a correlated random sampling technique applicable to gaussian random processes. The correlated sampling technique was developed by Hendrick and is described in Reference 9. A separate set of correlated gaussian random variables is generated for use in the representation of the focus component of the signal. The scintillating signal amplitudes and phases generated by this process are presented in Figures 15 and 16. The phase as plotted in Figure 15 is constrained to an interval ranging from -3π to 3π radians.. Whenever the actual phase decreases below -3π , 2π is added to all subsequent phase values and plotting continues. The many sharp discontinuities shown in Figure 15 are results of the addition of these 2π shifts and affect only the plotted phase, not the receiver.

The form of the MPS inputs to the receiver model is the same as that for experimental data. These are the signals presented in Figures 12 through 14.

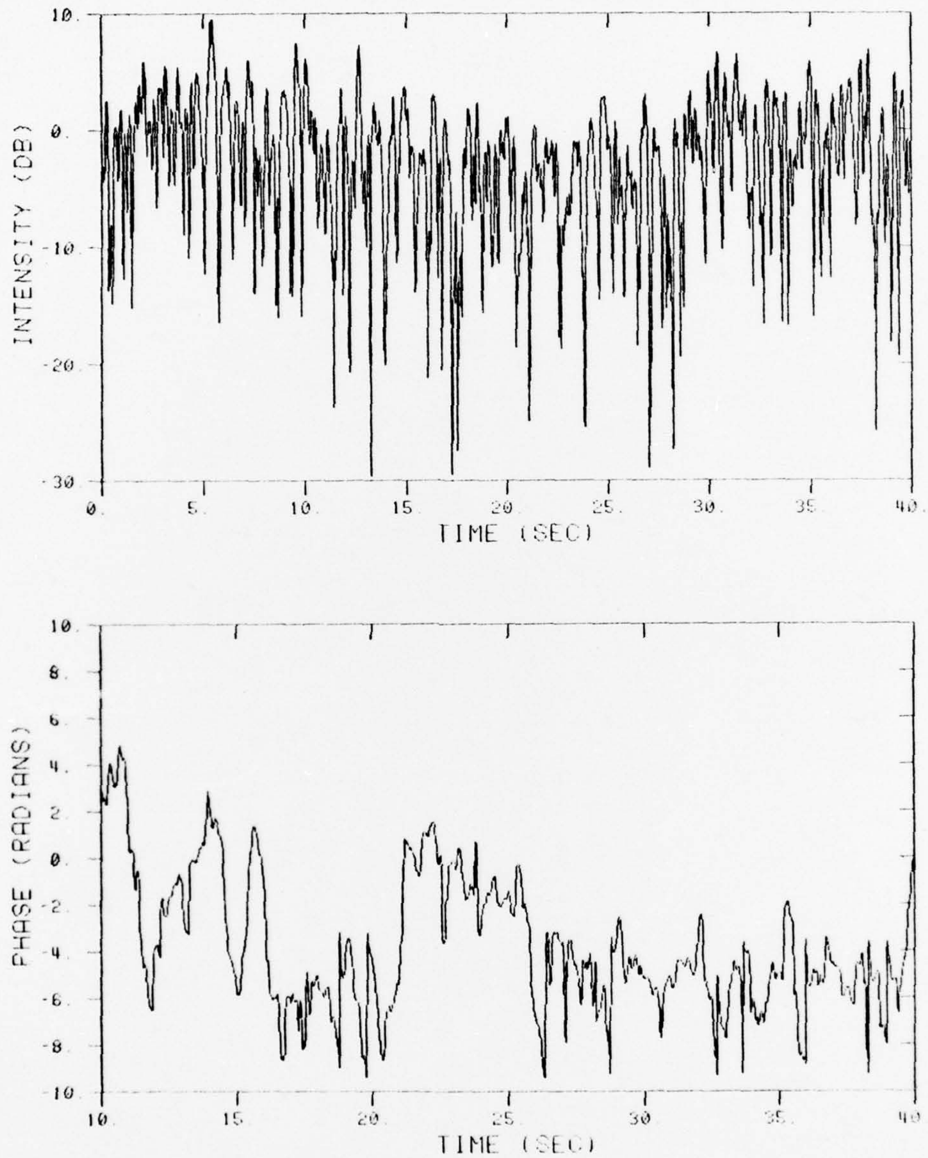

Figure 15. Simulated severely scintillating UHF signal using the 2-component model. (Compare with Figure 1.)

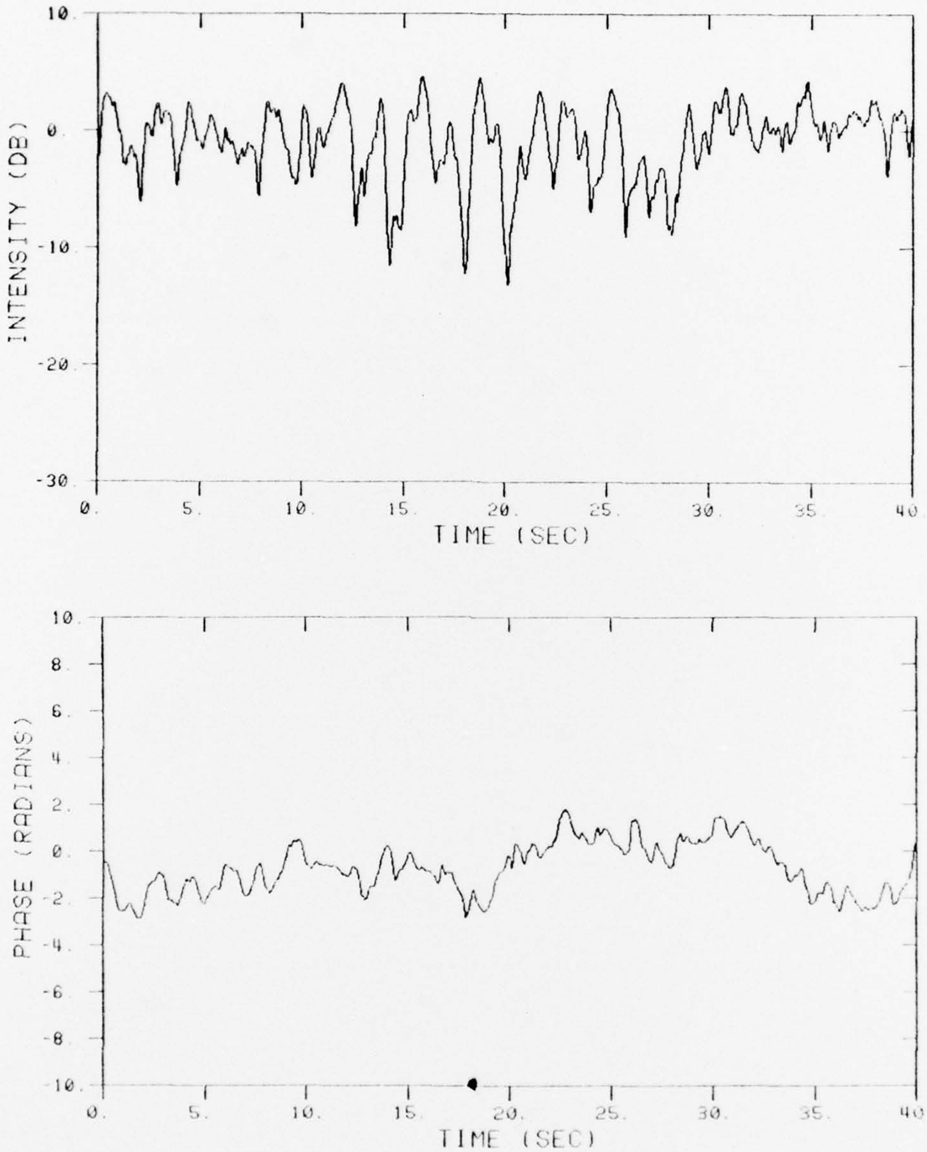

Figure 16. Simulated moderately scintillating UHF signal using the 2-component model. (Compare with Figure 2.)

SECTION 6
SIMULATION RESULTS

A phase shift keyed bit stream which carries the ASCII-coded message "Simulation of coherent PSK satellite communications during signal disturbances." is used here in the receiver model. The biphase modulated carrier is modified by the signal amplitude and phase perturbations from Wideband data, MPS calculations, or the 2-component model. The simulated receiver attempts to track the carrier in a Costas loop, adjust for amplitude variations with an AGC circuit, and coherently detect the data.

The following is an example of the message output from the receiver simulation using the severely scintillating UHF Wideband data samples.

```
WIMUMCTION OF COHERENT PSK SATELLITE COMMUNICATIONS DU ING SIGFAL DISTURBANCE /
SILUL+TION OF%COHARENT PSK SATELLITE COMMUJICATIO.S DUBING SIG AL  JSTURBANCES.
SIMULATION OF C<HERENT#PSK SATELLITE!COGMUNICAUI NS DURING SIGNAL DISTURBANCES.$
CIMWDATION  F COHERE T#PSK KATULLITE C<MMUNICATIONS DURIN  SIGNAL DISTURBANCES.
RIMULATION#MF COHERENT PSK SATELLITE COMMUNICATIONS DURING SIGNAL D STUR ANCES.
SIMUNATI N OF COHERENT PSK SA
```

Outputs using signals derived from the models for this time period look much the same with a different array of errors. Decoding errors are caused by phase tracking errors and phase slipping in the Costas loop, as well as by amplitude fades below the threshold for reliable data detection. A summary of binary error statistics from the simulations is given in Table 4.

Table 4. Summary of error statistics.

Mean E_b/N_o = 16.25 db

	Transmitted Bits	Demodulated Bit Errors	Calculated Average Bit Error Probability
<u>Severe Scintillation</u>			
UHF Wideband Data	3003	59	1.3×10^{-2}
2-Component Model	3003	67	2.3×10^{-2}
MPS Model	3003	55	2.0×10^{-2}
<u>Moderate Scintillation</u>			
Wideband Data	3003	1	2.2×10^{-5}
2-Component Model	3003	0	3.9×10^{-4}
MPS Model	3003	4	4.9×10^{-4}
<u>L-Band</u>			
Wideband Data	2254	0	2.1×10^{-6}
MPS Model	2254	2	8.9×10^{-4}

An explicit bit by bit demodulation process is simulated in the receiver model. In addition, a conditional binary error probability is calculated. The conditional error probability is a function of the phase tracking error and the signal amplitude at each sampling time. The calculated bit error rates given in Table 4 are computed by averaging the conditional binary error probabilities over the simulation time interval. These are the average error rates that would be expected for very long samples. When the average error probability is of the order of 10^{-4}, the expected number of bit errors in a 40 second period, for a bit rate of 75/sec, is less than one. However, because the decorrelation time is long compared to a bit period, the errors are clumped in time. Longer simulations would be required to obtain good statistics for demodulated bit errors in the cases involving moderate scintillation.

SECTION 7
CONCLUSIONS

Models for representation of radio signals that have propagated through a disturbed ionosphere are useful for generating input signals for computer simulation of communication systems. One of the models used here, the joint gaussian plus log normal 2-component model, represents the signal through measured statistical parameters. The second model, the multiple phase screen model, represents the signal by generating amplitude and phase samples based on physical propagation effects. In the comparison of these models presented here, a digital simulation of a BPSK demodulator was found to give similar demodulation performance for the two signal models. The binary error rates resulting from use of the models were comparable to results obtained from use of the data taken from the DNA Wideband satellite experiment.

In this work the MPS simulations which were obtained to "match" the Wideband satellite data were chosen on the basis of scintillation index and phase standard deviation from a small set of possible cases. Future work of this type should be directed toward matching the intensity and phase power spectral densities of the received signal to obtain a match of both first and second order statistics. In addition to being a further test of how well the models match experimental data, these quantities impose requirements on automatic gain control and phase tracking loop bandwidths.

The MPS technique has advantages for communication link simulations because the parameters required are related to ionospheric structure rather than a priori assumptions of signal statistics.

REFERENCES

1. Fremouw, E. J., R. L. Leadabrand, R. C. Livingston, M. D. Cousins, C. L. Rino, B. C. Fair, and R. A. Long, "Early Results from the DNA Wideband Experiment—Complex Signal Scintillation," Radio Science, Volume 13, No. 1, Jan-Feb 1978.

2. Paulson, M. R., and R. U. F. Hopkins, Effects of Equatorial Scintillation Fading of SATCOM Signals, NELC/TR 1875, Naval Electronics Laboratory Center, May 1973.

3. Taur, R. R., "Ionospheric Scintillation at 4 and 6 GHz," Comsat Technical Review, Volume 3, No. 1, pp. 145-163, Spring 1973.

4. Stevens, R. K., A Review of Satellite Signal Scintillation Observations and Research, ESL-TM421, ESL Incorporated, November 1973.

5. Fremouw, E. J., and C. L. Rino, Continued Modeling of Transionospheric Radio Propagation, Stanford Research Institute, August 1976.

6. Knepp, D. L., Multiple Phase-Screen Propagation Analysis for Defense Satellite Communications System, DNA 4424T, (MRC-R-332), Mission Research Corporation, September 1977.

7. Bogusch, R. L., F. W. Guigliano, D. L. Knepp, A. H. Michelet, and B. E. Sawyer, Propagation Effects on DSCS II Links, (unpublished).

8. Ratcliffe, J. H., "Some Aspects of Diffraction Theory and Their Application to the Ionosphere," Reports on Progress in Physics, The Physical Society, London, 1956.

9. Hendrick, R. W., On the Continuation of Gaussian Series, MRC-N-168, Mission Research Corporation, November 1974.

10. Wittwer, L. A., T. Salvi, and E. Pettus, UHF Propagation Effects in Scintillated Environments, AFWL-TR-76-304, Air Force Weapons Laboratory, August 1977.

DISTRIBUTION LIST

DEPARTMENT OF DEFENSE

Assistant Secretary of Defense
Comm, Cmd, Cont. & Intell.
ATTN: M. Epstein
ATTN: J. Babcock

Assistant to the Secretary of Defense
Atomic Energy
ATTN: Executive Assistant

Command & Control Technical Center
Department of Defense
ATTN: C-650, W. Heidig
ATTN: C-650, G. Jones
ATTN: C-312, R. Mason

Defense Advanced Rsch. Proj. Agency
ATTN: TIO

Defense Communication Engineer Center
ATTN: Code R410, J. McLean
ATTN: Code R720, J. Worhtington

Defense Communications Agency
ATTN: Code 810, J. Barna
ATTN: Code 480
ATTN: Code 101B
ATTN: Code R1033, M. Raffensperger

Defense Documentation Center
12 cy ATTN: DD

Defense Intelligence Agency
ATTN: DC-7D, W. Wittig
ATTN: HQ-TR, J. Stewart
ATTN: DB-4C, E. O'Farrell
ATTN: DT-1BZ, R. Morton
ATTN: DB, A. Wise
ATTN: DT-5
ATTN: DT-1B

Defense Nuclear Agency
ATTN: DDST
ATTN: STVL
3 cy ATTN: RAAE
4 cy ATTN: TITL

Field Commmand
Defense Nuclear Agency
ATTN: FCPR

Interservice Nuclear Weapons School
ATTN: TTV

Joint Chiefs of Staff
ATTN: J-3, WWMCCS Evaluation Office

Joint Strat. Tgt. Planning Staff
ATTN: JLTW-2
ATTN: JPST, G. Goetz

Livermore Division, Field Command, DNA
Lawrence Livermore Laboratory
ATTN: FCPRL

DEPARTMENT OF DEFENSE (Continued)

National Security Agency
Department of Defense
ATTN: B3, F. Leonard
ATTN: R52, J. Skillman
ATTN: W32, O. Bartlett

Under Secretary of Defense for Rsch. & Engrg.
ATTN: Strategic & Space Systems (OS)

WWMCCS System Engineering Org.
ATTN: R. Crawford

DEPARTMENT OF THE ARMY

Atmospheric Sciences Laboratory
U.S. Army Research & Development Command
ATTN: DELAS-AE-M, F. Niles

ERADCOM Technical Support Activity
Department of the Army
ATTN: DELET-ER, H. Bomke

Harry Diamond Laboratories
Department of the Army
ATTN: DELHD-N-TI, M. Weiner
ATTN: DELHD-N-NP, F. Wimenitz
ATTN: DELHD-N-RB, R. Williams
ATTN: DELHD-N-NP

U.S. Army Comm-Elec. Engrg. Instal. Agency
ATTN: CCC-EMEO-PED, G. Lane
ATTN: CCC-EMEO, W. Nair

U.S. Army Foreign Science & Tech. Ctr.
ATTN: DRXST-SD

U.S. Army Materiel Dev. & Readiness Command
ATTN: DRCLDC, J. Bender

U.S. Army Nuclear & Chemical Agency
ATTN: Library

U.S. Army Satellite Comm. Agency
ATTN: Document Control

DEPARTMENT OF THE NAVY

Naval Electronic Systems Command
ATTN: PME 117
ATTN: NAVALEX 034, T. Hughes
ATTN: Code 5011
ATTN: PME 117-T

Naval Intelligence Support Center
ATTN: NISC-50

Naval Ocean Systems Center
ATTN: Code 0230, C. Baggett
ATTN: Code 81, R. Eastman
3 cy ATTN: Code 532, W. Moler

Naval Surface Surveillance System
ATTN: CAPT J. Burton

DEPARTMENT OF THE NAVY (Continued)

Naval Research Laboratory
ATTN: Code 7550, J. Davis
ATTN: Code 5460
ATTN: Code 7555
ATTN: Code 7580
ATTN: Code 6701, J. Brown
ATTN: Code 6700, T. Coffey
ATTN: Code 7500, B. Wald

Naval Surface Weapons Center
ATTN: Code F31

Naval Surface Weapons Center
Dahlgren Laboratory
ATTN: Code DF-14, R. Butler

Navy Space Systems Activity
ATTN: A. Hazzard
ATTN: Code 52

Office of Naval Research
ATTN: Code 461
ATTN: Code 421
ATTN: Code 402
ATTN: Code 420

Office of the Chief of Naval Operations
ATTN: Op-604
ATTN: Op-941

Strategic Systems Project Office
Department of the Navy
ATTN: NSSP-2722, F. Wimberly
ATTN: NSP-2141

DEPARTMENT OF THE AIR FORCE

Aerospace Defense Command/DC
Department of the Air Force
ATTN: DC, Mr. Long

Aerospace Defense Command/XPD
Department of the Air Force
ATTN: XPDQQ
ATTN: XP

Air Force Avionics Laboratory
ATTN: AAD, W. Hunt
ATTN: AAD, A. Johnson

Air Force Geophysics Laboratory
ATTN: OPR-1, J. Ulwick
ATTN: PHP, J. Aarons
ATTN: LKB, K. Champion
ATTN: OPR, A. Stair
ATTN: PHD, J. Buchau
ATTN: PHD, J. Mullen

Air Force Technical Applications Center
ATTN: TF/Maj Wiley

Air Force Weapons Laboratory
ATTN: SUL
ATTN: DYC, J. Kamm
ATTN: DYC, J. Barry

Deputy Chief of Staff
Research, Development, & Acq.
Department of the Air Force
ATTN: AFRDQ

DEPARTMENT OF THE AIR FORCE (Continued)

Deputy Chief of Staff
Programs & Analyses
Department of the Air Force
ATTN: PACSC, Maj Paul

Electronic Systems Division, AFSC
ATTN: J. Whelan
ATTN: DCKC, J. Clark
ATTN: XRW, J. Deas
ATTN: YSEA

Foreign Technology Division, AFSC
ATTN: FTDP, B. Ballard
ATTN: NICD, Library

Rome Air Development Center, AFSC
ATTN: Documents Library/TSLD
ATTN: OCSE, V. Coyne

Rome Air Development Center, AFSC
ATTN: EEP

Space and Missile Systems Organization/SK
Air Force Systems Command
ATTN: SKA, M. Clavin

Strategic Air Command/XPFS
Department of the Air Force
ATTN: DOK, Chief Scientist
ATTN: NRT

DEPARTMENT OF ENERGY

Department of Energy
Albuquerque Operations Office
ATTN: Doc. Con. for D. Sherwood

Department of Energy
Library Room G-042
ATTN: Doc. Con. for A. Labowitz

Office of Military Application
Department of Energy
ATTN: Doc. Con. for D. Gale

OTHER GOVERNMENT AGENCIES

Central Intelligence Agency
ATTN: RD/SI, Rm. 5G48, Hq. Bldg.
for OSI/PSTD

Department of Commerce
National Bureau of Standards
ATTN: R. Moore

Department of Transportation
Office of the Secretary
ATTN: R. Doherty
ATTN: R. Lewis

Institute for Telecommunications Sciences
National Telecommunications & Info. Admin.
ATTN: W. Utlaut
ATTN: D. Crombie
ATTN: L. Berry
ATTN: A. Dean

OTHER GOVERNMENT AGENCIES (Continued)

National Oceanic & Atmospheric Admin.
Environmental Research Laboratory
Department of Commerce
ATTN: G. Reid
ATTN: R. Grubb

DEPARTMENT OF DEFENSE CONTRACTORS

Aerospace Corporation
ATTN: I. Garfunkel
ATTN: SMEA for PWW
ATTN: S. Bower
ATTN: F. Morse
ATTN: V. Josephson
ATTN: T. Salmi
ATTN: J. Carter
ATTN: N. Stockwell
ATTN: D. Olsen

Analytical Systems Engineering Corp.
ATTN: Radio Sciences

Berkeley Research Associates, Inc.
ATTN: J. Workman

Boeing Company
ATTN: G. Hall
ATTN: D. Murray
ATTN: G. Keister
ATTN: J. Kenney

Brown Engineering Company, Inc.
ATTN: R. Deliberis

University of California at San Diego
ATTN: H. Booker

Charles Stark Draper Lab., Inc.
ATTN: J. Gilmore
ATTN: D. Cox

Computer Sciences Corporation
ATTN: H. Blank

COMSAT Labs.
ATTN: G. Hyde
ATTN: R. Taur

Cornell University
Department of Electrical Engineering
ATTN: D. Farley, Jr.

Electrospace Systems, Inc.
ATTN: H. Logston

ESL, Inc.
ATTN: J. Marshall
ATTN: C. Prettie
ATTN: J. Roberts

Ford Aerospace & Communications Corporation
ATTN: J. Mattingley

General Electric Company
Space Division
ATTN: M. Bortner

DEPARTMENT OF DEFENSE CONTRACTORS (Continued)

General Electric Company
ATTN: F. Reibert

General Electric Co.-TEMPO
Center for Advanced Studies
ATTN: W. Knapp
ATTN: DASIAC
ATTN: T. Stevens
ATTN: D. Chandler
ATTN: M. Stanton

General Electric Tech. Services Co., Inc.
ATTN: G. Millman

General Research Corporation
Santa Barbara Division
ATTN: J. Ise, Jr.
ATTN: J. Garbarino

Geophysical Institute
University of Alaska
ATTN: N. Brown
ATTN: T. Davis
ATTN: Technical Library

GTE Sylvania, Inc.
Electronics Systems Grp.-Eastern Div.
ATTN: M. Cross

HSS, Inc.
ATTN: D. Hansen

University of Illinois
Department of Electrical Engineering
ATTN: K. Yeh

Institute for Defense Analyses
ATTN: J. Aein
ATTN: J. Bengston
ATTN: E. Bauer
ATTN: H. Wolfhard

International Tel. & Telegraph Corporation
ATTN: Technical Library

JAYCOR
ATTN: S. Goldman

Johns Hopkins University
Applied Physics Lab.
ATTN: Document Librarian
ATTN: T. Potemra

Kaman Sciences Corporation
ATTN: T. Meagher

Lawrence Livermore Laboratory
University of California
ATTN: Doc. Con. for Tech. Info. Dept. Library
ATTN: Doc. Con. for L-46, F. Seward

Linkabit Corporation
ATTN: T. Jacobs

Lockheed Missiles & Space Co., Inc.
ATTN: Dept. 60-12
ATTN: D. Churchill

DEPARTMENT OF DEFENSE CONTRACTORS (Continued)

Lockheed Missiles and Space Co., Inc.
ATTN: W. Imhof
ATTN: M. Walt
ATTN: R. Johnson

Los Alamos Scientific Laboratory
ATTN: Doc. Con. for P. Keaton
ATTN: Doc. Con. for D. Westervelt
ATTN: Doc. Con. for R. Taschek

M.I.T. Lincoln Laboratory
ATTN: D. Towle
ATTN: L. Loughlin
ATTN: P. Waldron
ATTN: D. Clark

McDonnell Douglas Corporation
ATTN: W. Olson
ATTN: G. Mroz
ATTN: J. Moule
ATTN: N. Harris

Mission Research Corporation
ATTN: R. Scott
ATTN: D. Knepp
ATTN: M. Scheibe
ATTN: D. Sowle
ATTN: F. Fajen
ATTN: R. Bogusch
ATTN: R. Hendrick
ATTN: S. Gutsche
5 cy ATTN: Document Control

Mitre Corporation
ATTN: C. Callahan
ATTN: G. Harding

Mitre Corporation
ATTN: M. Horrocks
ATTN: W. Foster
ATTN: W. Hall

Pacific-Sierra Research Corporation
ATTN: E. Field, Jr.

Pennsylvania State University
ATTN: Ionospheric Research Lab.

Photometrics, Inc.
ATTN: I. Kofsky

Physical Dynamics, Inc.
ATTN: E. Fremouw

R & D Associates
ATTN: C. MacDonald
ATTN: F. Gilmore
ATTN: W. Wright, Jr.
ATTN: W. Karzas
ATTN: R. Lelevier
ATTN: R. Turco
ATTN: H. Ory
ATTN: B. Gabbard

Rand Corporation
ATTN: C. Crain
ATTN: F. Bedrozian

DEPARTMENT OF DEFENSE CONTRACTORS (Continued)

Sandia Laboratories
Livermore Laboratory
ATTN: Doc. Con. for B. Murphey
ATTN: Doc. Con. for T. Cook

Sandia Laboratories
ATTN: Doc. Con. for Space Project Div.
ATTN: Doc. Con. for D. Thornbrough
ATTN: Doc. Con. for D. Dahlgren
ATTN: Doc. Con. for 3141
ATTN: Doc. Con. for W. Brown

Science Applications, Inc.
ATTN: D. Sachs
ATTN: L. Linson
ATTN: D. Hamlin

Science Applications, Inc.
Huntsville Division
ATTN: D. Divis

Science Applications, Inc.
ATTN: SZ

SRI International
ATTN: G. Price
ATTN: A. Burns
ATTN: G. Smith
ATTN: C. Rino
ATTN: D. Neilson
ATTN: W. Chesnut
ATTN: G. Carpenter
ATTN: M. Baron
ATTN: W. Jaye
ATTN: R. Livingston
ATTN: R. Leadabrand

Tri-Com, Inc.
ATTN: D. Murray

TRW Defense & Space Sys. Group
ATTN: S. Altschuler
ATTN: R. Plebuch
ATTN: D. Dee

Utah State University
Center for Research in Aeronomy
Space Science Laboratory, UMC-41
ATTN: K. Baker
ATTN: L. Jensen

Visidyne, Inc.
ATTN: J. Carpenter

Riverside Research Institute
ATTN: V. Trapani